Available online at www.sciencedirect.com
SCIENCE DIRECT®
Polymer 44 (2003) 7199–7208
polymer
www.elsevier.com/locate/polymer

Modeling of the viscoelastic behavior of amorphous polymers by the differential and integration fractional method: the relaxation spectrum $H(\tau)$

Mataz Alcoutlabi[a,*], J.J. Martinez-Vega[b,c]

[a]*Department of Chemical Engineering, Texas Tech. University, 6th and Canton, Lubbock, TX 79409-3121, USA*
[b]*Laboratoire Matériaux Organique à Proprietés Spésifiques UMR 5041 CNRS-Université de Savoie, Bat. IUT, Campus Scientifique, Le Bourget du Lac 73376, France*
[c]*Laboratoire de Génie Electrique (UMR-CNRS 5003), Université Paul Sabatier, 118 route de Narbonne, Toulouse Cedex 31062, France*

Received 1 April 2003; received in revised form 14 August 2003; accepted 22 August 2003

Abstract

The dynamic mechanical behavior of poly(methyl methacrylate) (PMMA) from deep in the glass to the glass transition region has been studied by DMTA and analyzed by using a phenomenological fractional model in which the dynamic stress appears as a non-integer-order derivative of the strain. In order for the model to accurately represent the experimental data, three non-integer values for the derivative order are required. These values are related to two relaxation mechanisms. In the low temperature region (i.e. the β relaxation of PMMA), the derivative order is smaller and near 0.2, which indicates behavior close to the ideal elastic solid (glassy). For higher temperatures (between the β and the α relaxations), the derivative order is higher, indicating more viscoelastic behavior. In this work, modeling of the viscoelastic behavior of polymers using the fractional calculus approach is presented and the extended fractional solid (EFS) model is used to fit the experimental data of PMMA. In addition, the continuous relaxation spectrum $H(\tau)$ of PMMA is calculated from the model using the inverse Stieljes integral transformation. Finally, the effect of thermal treatment on the non-integer model parameters and on the distribution of relaxation times is obtained.

Keywords: Fractional calculus; Poly(methyl methacrylate)-viscoelasticity; Physical aging

1. Introduction

In recent years, there has been a considerable amount of work carried out on modeling the viscoelastic response of polymer materials [1,2] over a wide range of temperature (T) and time (t) or frequency (f). These investigations deal primarily with the modeling (or fitting) of various viscoelastic functions. These functions can be described by the generalized Maxwell model or the generalized Kelvin–Voigt model [1]. Using these models to fit the data obtained in relaxation or creep experiments of amorphous polymers requires the determination of a number of fitting parameters.

An alternative approach has been used to model the viscoelastic behavior of polymers that is based on the concept of the differential and integral fractional method [3–19]. The method uses the idea that the spring and dashpot elements in the phenomenological models are replaced by a spring-pot element [7]. The advantage of this method is that it reduces the number of fitting parameters used to model the viscoelastic behavior of polymers. For example, in relaxation experiments, the relationship between the resulting stress $\sigma(t)$ and the applied strain $\varepsilon(t)$ (using the spring-pot element) is dependent on the fractional derivative of order a of the applied strain where a is between 0 and 1.

$$\sigma(t) = E\tau^a \frac{\mathrm{d}^a \varepsilon(t)}{\mathrm{d}t^a} \tag{1}$$

Note that the spring-pot element is equivalent to a pure spring element if the parameter $a = 0$ and is equivalent to a pure dashpot element if $a = 1$.

The use of fractional calculus was introduced some time

* Corresponding author. Tel.: +1-806-7420448; fax: +1-806-7423552.
E-mail address: mataz.alcoutlabi@coe.ttu.edu (M. Alcoutlabi).

0032-3861/$ - see front matter © 2003 Elsevier Ltd. All rights reserved.
doi:10.1016/j.polymer.2003.08.036

ago in describing general viscoelastic behavior [4]. Bagley and Torvik [4] showed that the low frequency characteristics of the Rouse model could be retrieved using a fractional differential equation of order 0.5. Friedrich [8], and Glöckle and Nonnenmacher [10] modified the Zener model by replacing the regular derivatives by fractional derivatives. The relaxation modulus calculated from this model is a monotonically decreasing function of time. The response was obtained by establishing parameter combinations to ensure thermodynamic compatibility of the solution [8,10]. It was also shown by Heymans and Bauwens [11] that fractional order equations obtained from such models automatically fulfilled the thermodynamic compatibility conditions given by Friedrich [8] and Glöckle and Nonnenmacher [10].

Schiessel and Blumen [12,13], Heymans and Bauwens [11] and Heymans [15] have demonstrated that the differential equation of the spring-pot element given above can be realized physically through hierarchical arrangements of springs and dashpots, such as ladders, trees and fractal networks. In the limit of an infinite number of constitutive elements these arrangements obey Eq. (1). Schiessel and Blumen [12] showed that the spring-dashpot ladder with equal spring constants and viscosities obeys Eq. (1). Heymans and Bauwens [12] also showed that the self-similar hierarchical tree model can obey Eq. (1) for equal spring constants and viscosities. In addition, the self-similar tree model can be generalized to yield any exponent a between 0 and 1. This generalization is required, for example, if interchain forces are viscoelastic rather than purely viscous [11]. Moreover, Schiessel and Blumen [12] have shown that fractal arrangements of identical springs and dashpots (e.g. a Sierpinski gasket) lead to an exponent a which is linked to the spectral dimension of the fractal arrangement. It has also been shown that molecular processes governed by continuous time random walks with Levy-type waiting time distributions lead to constitutive equations with fractional derivatives [16]. It was also found that generalized fractional time derivatives of order a arise naturally in the transition between microscopic and macroscopic time scales [5].

Recently, Hilfer published several papers concerning the fractional calculus method and its application to fitting the dielectric data of glass forming liquids [17,18] and of propylene carbonate [19]. In that work, Hilfer introduced a novel fitting function for the complex frequency-dependent dielectric susceptibility [17]. This function was compared with other fitting functions for experimental broad band dielectric loss spectra. The fitting function contains a single stretched exponent, similar to the familiar Cole–Davidson [20] or Kohlrausch-Williams-Watt [21] stretched exponential fits. The function of Hilfer was compared to these traditional fits as well as to the Havriliak-Negami [22] susceptibility and susceptibility for two-step Debye relaxation. The results of Hilfer's fit were found to give superior agreement. Also, Hilfer [19] solved the differential equation for composite fractional relaxation and used the resulting dynamical susceptibility function to fit the broad band dielectric spectroscopy data of glycerol. In that work, qualitative and quantitative agreement with the dielectric data was found. The fits required fewer parameters than traditional fit functions and can extend over 13 decades in frequency. For more detail on the application of fractional calculus in physics, an extensive review can be found in reference [5].

The objective of this paper is to present a fractional calculus model to describe the viscoelastic behavior of poly(methyl methacrylate) (PMMA) over a wide temperature range from the glassy to the glass transition region. The viscoelastic behavior of PMMA in this temperature range cannot be represented by the Cole–Cole equation [23–25] due to the existence of a broad secondary β relaxation at room temperature. In addition, the effect of thermal history on the model parameters and on the relaxation time spectra $H(\tau)$ is also investigated.

2. Fractional calculus modeling

2.1. The extended fractional solid model (EFS)

Here, we start with the three-element Zener model, consisting of a spring and a dashpot in series (Maxwell element) with a spring in parallel. The stress $\sigma(t)$–strain $\varepsilon(t)$ relationship of the standard Zener model is given by the first-order differential equation:

$$\sigma(t) + \tau\frac{\mathrm{d}\sigma(t)}{\mathrm{d}t} = E_0\tau\frac{\mathrm{d}\varepsilon(t)}{\mathrm{d}t} + (E_1 - E_0)\varepsilon(t) \tag{2}$$

where $\tau = (E_1 - E_0)/\eta$ is a characteristic relaxation time. The Fractional Zener model [7] can be obtained from Eq. (2) by replacing the first order derivative $\mathrm{d}/\mathrm{d}t$ by a differential order $\mathrm{d}^a/\mathrm{d}t^a$. This is equivalent to replacing the dashpot element with a spring-pot element given by Eq. (1). The EFS model that we developed in our previous work [24] consists of two fractional models in parallel (Fig. 1). The first one is the fractional Zener model with one spring-pot FZ_1 and the second one is the Fractional Zener model with two spring-pots FZ_2. Therefore, the relaxation modulus calculated from the EFS can be expressed as:

$$E(t) = E_{FZ_1}(t) + E_{FZ_2}(t) \tag{3}$$

where E_{FZ_1} is the relaxation modulus calculated from FZ_1 and E_{FZ_2} is the relaxation modulus calculated from FZ_2. The dynamic modulus $E^*(\mathrm{i}\omega)$ calculated from the EFS model can be obtained by applying the Fourier transform to Eq. (3),

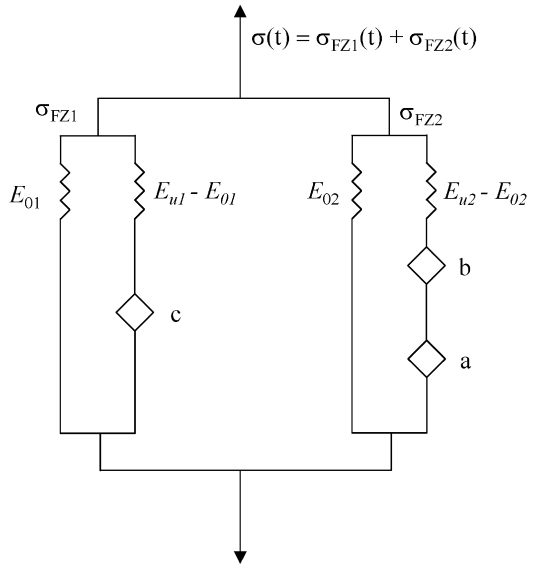

Fig. 1. The extended fractional solid (EFS) model.

giving:

$$E^*(\mathrm{i}\omega) = \frac{E_{0_2} + E_{\mathrm{u}_1}(\mathrm{i}\omega\tau_c)^c}{1 + (\mathrm{i}\omega\tau_c)^c} + \frac{E_{0_2} + E_{\mathrm{u}_2}[(\mathrm{i}\omega\tau_a)^{-a} + (\mathrm{i}\omega\tau_b)^{-b}]}{1 + (\mathrm{i}\omega\tau_a)^{-a} + (\mathrm{i}\omega\tau_b)^{-b}} \quad (4)$$

where ω is the angular frequency, E_{0_1} and E_{u_1} are the relaxed and non-relaxed moduli associated with FZ_1, E_{0_2} and E_{u_2} are the relaxed and non-relaxed moduli associated with FZ_2. τ_c, τ_a and τ_b are characteristic relaxation times, a, b and c are non-integer fractional parameters whose values are between 0 and 1 where $1 \geq b \geq a \geq c > 0$. The storage modulus thus becomes:

$$E' = E_{0_1}\frac{(1+k)(\omega\tau_c)^{2c} + (\omega\tau_c)^c(2+k)\cos\left(c\frac{\pi}{2}\right) + 1}{\left[1 + (\omega\tau_c)^c\cos\left(c\frac{\pi}{2}\right)\right]^2 + \left[(\omega\tau_c)^c\sin\left(c\frac{\pi}{2}\right)\right]^2} + E_{0_2} + \frac{(E_{\mathrm{u}_2} - E_{0_2})(1+B_1)}{(1+B_1)^2 + B_2^2} \quad (5)$$

and the loss modulus is:

$$E'' = E_{0_1}\frac{k(\omega\tau_c)^c\sin\left(c\frac{\pi}{2}\right)}{\left[1 + (\omega\tau_c)^c\cos\left(c\frac{\pi}{2}\right)\right]^2 + \left[(\omega\tau_c)^c\sin\left(c\frac{\pi}{2}\right)\right]^2} + \frac{(E_{\mathrm{u}_2} - E_{0_2})B_2}{(1+B_1)^2 + B_2^2} \quad (6)$$

where:

$$B_1 = \theta(\omega\tau_a)^{-b}\cos\left(b\frac{\pi}{2}\right) + (\omega\tau_a)^{-a}\cos\left(a\frac{\pi}{2}\right)$$

$$B_2 = \theta(\omega\tau_a)^{-b}\sin\left(b\frac{\pi}{2}\right) + (\omega\tau_a)^{-a}\sin\left(a\frac{\pi}{2}\right)$$

$$\theta = \left(\frac{\tau_b}{\tau_a}\right)^{-b}$$

and

$$k = \frac{E_{\mathrm{u}_2} - E_{0_2}}{E_{0_2}}$$

2.2. The viscoelastic response of the EFS model

The EFS model calculation (Eqs. (5) and (6)) is presented in Figs. 2 and 3. The model parameters used for the calculation are listed in Table 1.

Fig. 2(a) and (b) show respectively, the storage and loss moduli as a function of frequency. These Figures show the contribution of the fractional Zener models FZ_1 and FZ_2. It

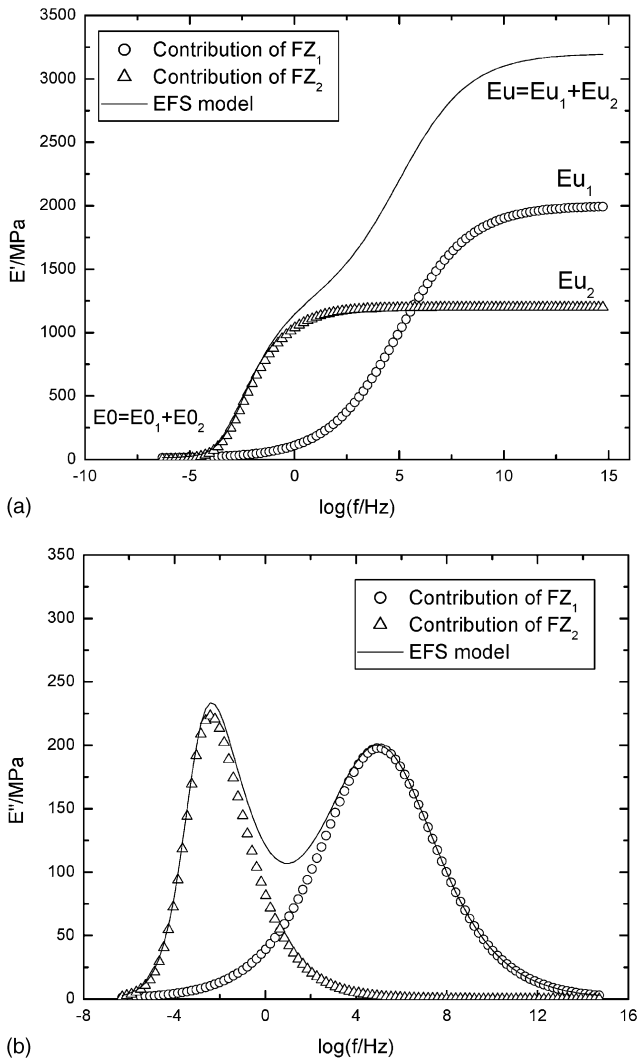

Fig. 2. (a) The ESF model calculation of the storage modulus $E'(f)$ from Eq. (5). (b) The ESF model calculation of the loss modulus $E''(f)$ from Eq. (6).

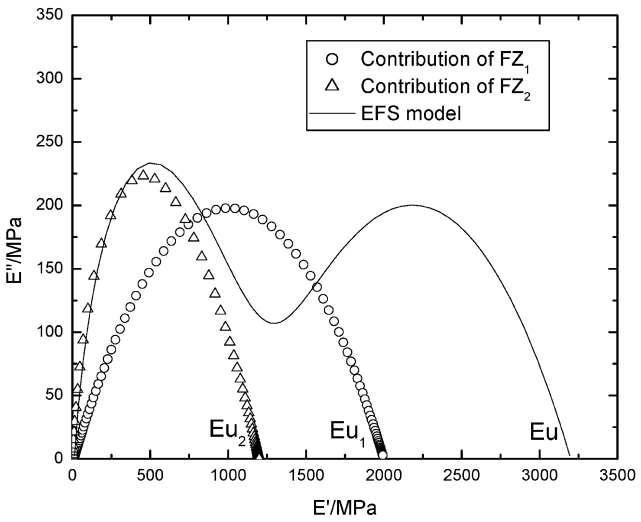

Fig. 3. The Cole–Cole diagram (E'' vs. E') for the ESF model.

is clear that the loss modulus calculated from the EFS model resulting from the two contributions show two maxima indicating the existence of two relaxations inherent in this model. Fig. 3 shows the Cole–Cole diagram corresponding to Fig. 2. Again, we can see the individual contribution of the FZ_1 and FZ_2 models. In addition, we have shown previously that the FZ_1 model displays Cole–Cole behavior [25] describing a single symmetrical peak independent of the value of the non-integer parameter c (c is related to the slope of the Cole–Cole diagram as shown below). The FZ_2 model describes an asymmetrical peak dependent on the parameters a and b [23]. Based on Fig. 2(a), we can see that the relaxed and non-relaxed moduli E_0 and E_u of the EFS model result from the individual contributions of the FZ_1 and FZ_2 models (i.e. $E_u = E_{u_1} + E_{u_2}$ and $E_0 = E_{0_1} + E_{0_2}$). The determination of the model parameters needed to fit the experimental data is discussed below.

We see then, that this model can represent the viscoelastic behavior of polymers showing two transitions such as α and β relaxations. We have shown previously [24] that the EFS model is a very good representation of the experimental data of PMMA from $T_g - 200\,^{\circ}C$ to $T_g + 15\,^{\circ}C$ and a good agreement was obtained between the model and the experimental data.

Table 1
The model parameters used in Figs. 2–4

a	0.33
b	0.79
c	0.25
E_{0_1} (MPa)	10
E_{0_2} (MPa)	1
E_{u_1} (MPa)	2000
E_{u_2} (MPa)	1200
τ_a (s)	200
τ_b (s)	600
τ_c (s)	1×10^{-5}

2.3. The relaxation spectrum $H(\tau)$

The relaxation spectrum $H(\tau)$ corresponding to the EFS model can be calculated by using the properties of the inverse Stieljes integral transformation [2]:

$$H(\tau) = \pm \mathrm{Im}\left\{ [E^*_{FZ_1}(s) + E^*_{FZ_2}(s)]_{s=\left(\frac{1}{\tau}\right)} e^{\mp i\pi} \right\}$$

$$= H_{FZ_1}(\tau) + H_{FZ_2}(\tau) \tag{7}$$

This spectrum can be obtained from Eqs. (7) and (4) in explicit form:

$$H(\tau) = \frac{E_{u_1} - E_{0_1}}{\pi} \left[\frac{\sin(c\pi)}{\left[\left(\frac{\tau}{\tau_c}\right)^c + \cos(c\pi) + \left(\frac{\tau}{\tau_c}\right)^{-c} \right]} \right]$$

$$+ \frac{E_{u_2} - E_{0_2}}{\pi} \left[\frac{B_2}{(1+B_1)^2 + B_2^2} \right] \tag{8}$$

where:

$$B_1 = \left(\frac{\tau}{\tau_a}\right)^a \cos(a\pi) + \theta \left(\frac{\tau}{\tau_a}\right)^b \cos(b\pi) \tag{9}$$

$$B_2 = \left(\frac{\tau}{\tau_a}\right)^a \sin(a\pi) + \theta \left(\frac{\tau}{\tau_a}\right)^b \sin(b\pi)$$

$$\theta = \left(\frac{\tau_b}{\tau_a}\right)^{-b}$$

Fig. 4 shows the relaxation spectrum $H(\tau)$, calculated from Eq. (8), as a function of the relaxation time τ for the same parameters listed in Table 1. This Figure shows the contribution of the spectra $H_{FZ_1}(\tau)$ and $H_{FZ_2}(\tau)$ calculated from FZ_1 and FZ_2 models, respectively. The shape of the

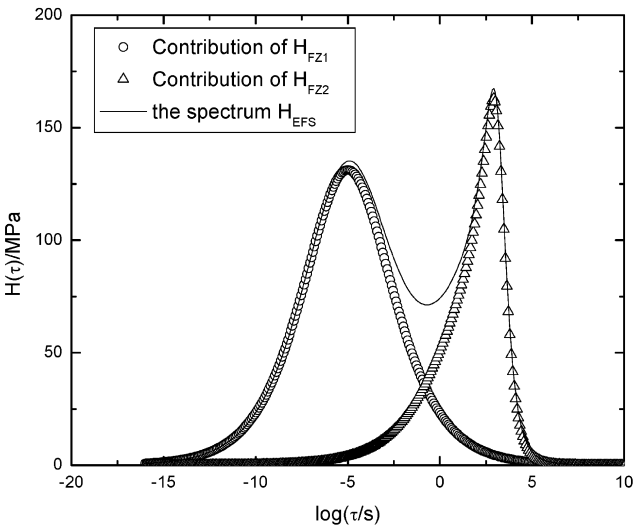

Fig. 4. The relaxation spectrum $H(\tau)$ calculated from ESF model using Eqs. (8) and (9). The model parameters used to calculate $H(\tau)$ are listed in Table 1.

spectrum shown in Fig. 4 is somewhat similar to that of the loss modulus shown in Fig. 2(b). The spectrum $H(\tau)$ shows two maxima, which are associated with the secondary and main relaxations for an amorphous polymer. Hence, this spectrum can represent the distribution of relaxation times of polymers characterized by a broad β relaxation.

Fig. 5 shows the spectrum $H(\tau)$ of the EFS model as a function of the relaxation time τ, calculated from Eq. (8), for different values of the non-integer parameters a, b and c. For a constant value of the a and c parameters and different values of b parameter (Fig. 5(a)), the b non-integer parameter affects mainly the longer time region of the spectrum (i.e. the main α relaxation for amorphous polymers). It can be seen in Fig. 5(b) that for constant values of b and c parameters, the a parameter affects mainly the neighborhood of the second maximum of the spectrum. Finally, we can see in Fig. 5(c) that the c parameter can affect the width of the spectrum, though the main effect is observed in the shortest relaxation time region (i.e. the first maximum associated with the β relaxation).

Thus, from Fig. 5, we can see that by appropriate manipulation of the parameters a, b and c, the $H(\tau)$ spectrum can represent the relaxation mechanism for complex systems or polymers characterized by two relaxations, the principal α relaxation and the secondary β relaxation. This is discussed below in the modeling section.

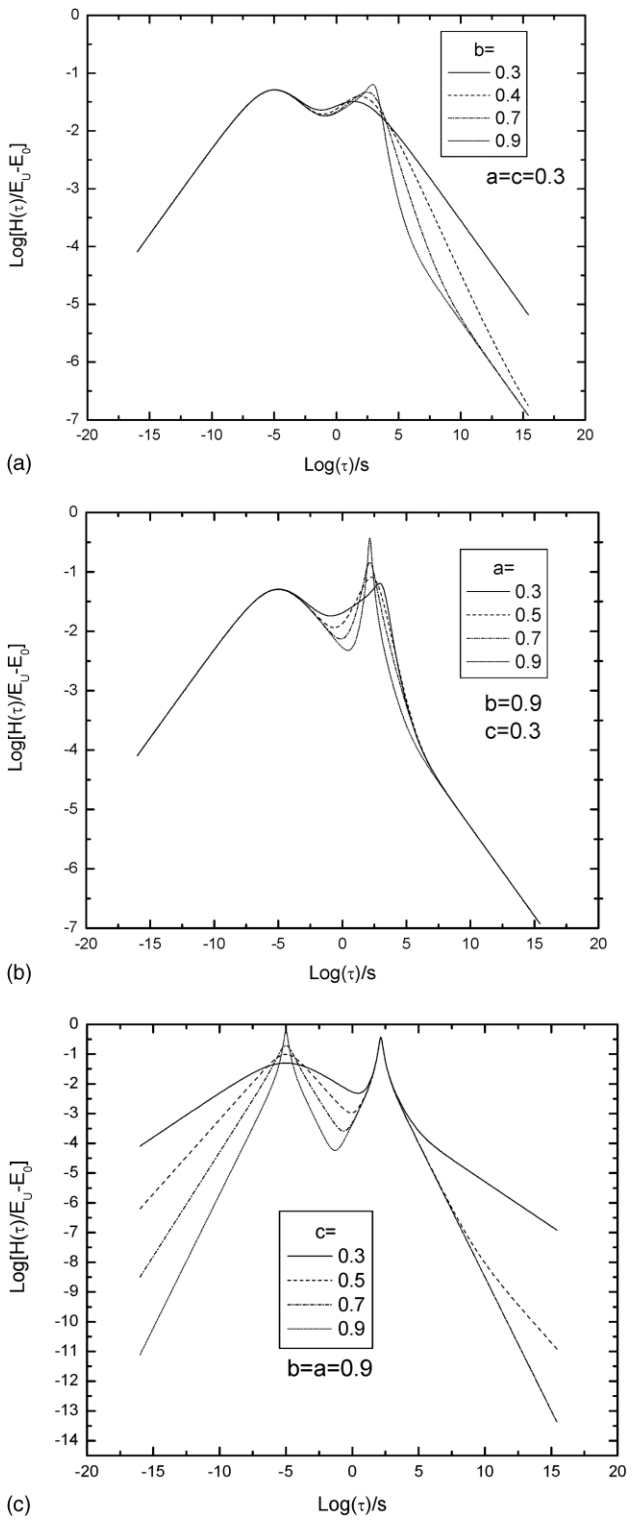

Fig. 5. The normalized relaxation spectrum $H(\tau)$ determined from ESF model for three cases. (a) $H(\tau)$ for a constant value of a and c parameters and different values of b parameters. (b) $H(\tau)$ for a constant value of b and c parameters and different values of a parameters. (c) $H(\tau)$ for a constant value of a and b parameters and different values of c parameters.

3. Experimental

3.1. Materials

Samples of PMMA were obtained from ELF, France who prepared and characterized them. The molecular weight, M_w, was determined to be 3×10^6 g/mol and polydispersity to be 2.3.

3.2. Dynamic mechanical measurements

Dynamic mechanical measurements were performed by using a DMTA MKIII (Rheometric Scientific) operating in double cantilever bending mode. The viscoelastic spectra were recorded from -80 to 130 °C, at a heating rate of 1 °C/min. The experiments were performed under isochronal conditions at a frequency of 1 Hz. The sample was approximately 2.4 mm thick, 6 mm wide and 35 mm long. This material had a measured T_g of 115 °C, as determined from differential scanning calorimetric measurements at a heating rate of 10 °C/min after cooling from 150 °C to ambient temperature at 10 °C/min.

3.3. Thermal treatments of the sample

Thermal treatments were performed as follows: the sample was placed in an oven and heated from room temperature to 80 °C, then dried for 1 h under vacuum. The

sample was further heated to 130 °C and then kept for 1 h under vacuum in order to erase the thermo-mechanical history and to dry the sample. After these treatments, the sample was immediately placed in the DMTA and cooled under nitrogen atmosphere to −80 °C and then the first DMTA run of the sample was performed from −80 to 130 °C ($T_g + 15$ °C). This is the reference sample. After the first DMTA run, the sample was cooled down (without removing it from the DMTA chamber) to the aging temperature of 70 °C and the aging process performed for 20 h. The sample was then cooled under nitrogen atmosphere to −80 °C and the second DMTA run was recorded up to $T_g + 15$ °C.

3.4. Data presentation

Most rheological data for polymers are presented in the form of the real and imaginary parts of the dynamic modulus or viscosity as a function of the frequency. A slightly different type of presentation is given by the Cole–Cole plot [23]. Another way to present the same rheological properties is to plot data for the phase angle $\delta(\omega, T)$ vs. the dynamic modulus $E^*(\omega, T)$, both measured at various frequencies and temperatures (denoted δ vs. E^* plots). These parameters constitute the primary experimental data, which relate to the storage and loss moduli in the following way:

$$\delta(\omega, T) = \left[\tan^{-1}\left(\frac{E''(\omega, T)}{E'(\omega, T)}\right)\right] \tag{10}$$

$$E^*(\omega, T) = \sqrt{[E'(\omega, T)]^2 + [E''(\omega, T]^2} \tag{11}$$

One reason why we chose to use this type of plot is that no additional data manipulation is required. Both δ and E^* are frequency and temperature dependent quantities, and the two quantities are related to each other by a simple relationship [26]:

$$\delta(\omega, T) \approx \frac{\pi}{2}\left[\frac{\mathrm{d}\ln E^*(\omega, T)}{\mathrm{d}\ln \omega}\right] \tag{12}$$

While the dynamic modulus E^* is quite insensitive to small changes in rheology, the phase angle δ is a very sensitive parameter because the phase angle is approximately the derivative of log $E^*(\omega)$ at different frequencies under isothermal conditions. Thus, we chose two different ways (the Cole–Cole and δ vs. E^* plots) to compare the experimental data of PMMA with the model calculation.

4. Results

Here we present some experimental data for PMMA over a wide range of temperature and at a frequency of 1 Hz. Fig. 6(a) and (b) show the loss moduli and tan δ of PMMA for the reference and aged samples as a function of temperature at 1 Hz. The temperature range is from −80 to 130 °C. Fig.

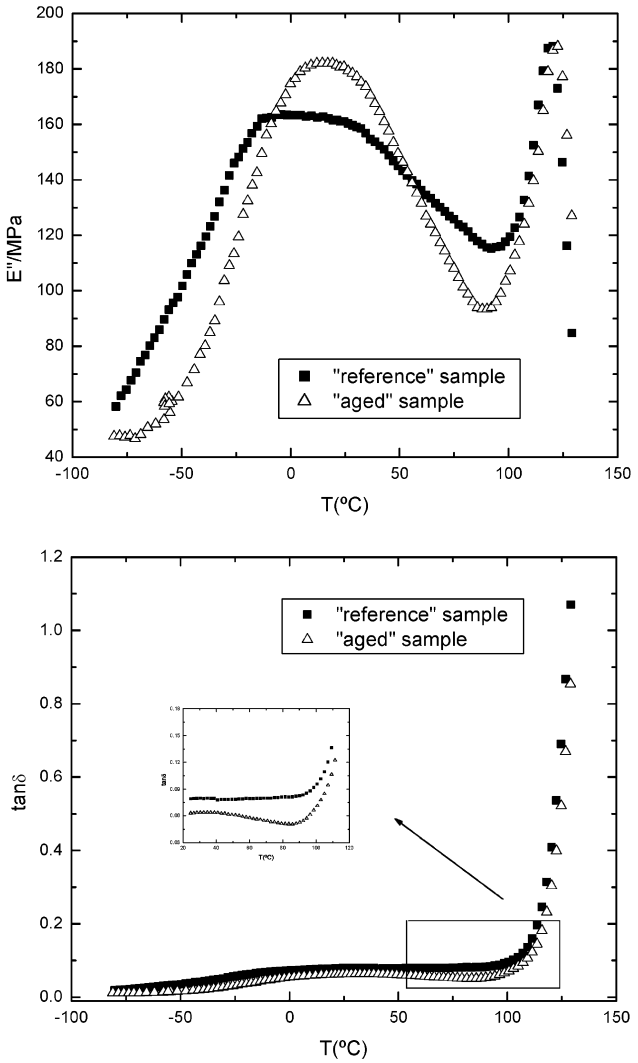

Fig. 6. (a) Loss modulus $E''(T)$ vs. temperature at a frequency of 1 Hz for the reference and aged sample of PMMA. (b) Loss factor tan δ vs. temperature at a frequency of 1 Hz for the reference and aged samples of PMMA.

7 shows the Cole–Cole diagram corresponding to Fig. 6(a) and (b). In low temperature range of Fig. 6(a), the broad β secondary relaxation, which is characteristic of this polymer, is clearly observable. The broadness of the β relaxation peak could be due to a superposition of many relaxation mechanisms. Based on the analysis of mechanisms associated with physical aging phenomenon, the molecular mobility is the fundamental property being affected by this phenomenon [27]. The dynamic modulus is a rheologic property, which reflects the molecular mobility of polymers. It is known that the effect of physical aging is to reduce the molecular mobility and so measurements of the dynamic modulus can give information about the effect of any thermal treatment or physical aging on the molecular mobility. The experimental data presented in Fig. 6(a) and (b) show that the physical aging process affects the region below the α relaxation of PMMA. In the high temperature region, above T_α, the material

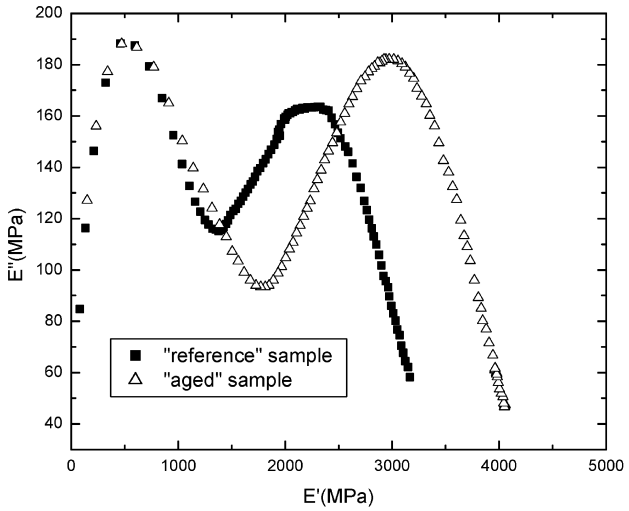

Fig. 7. Comparison in the complex plane between the reference and the aged samples.

reaches the thermodynamic equilibrium and no physical aging effect was observed. However, in the low temperature region, below T_β, the molecular mobility is too slow and no physical aging effect can be observed in this region during the time scale of the experiment.

This is classical physical aging behavior, and is similar to that reported in the literature, for the same material in studying the isochronal response by dynamic mechanical measurements [28–29]. It is important to note that the relaxation spectrum of the aged material will move to longer relaxation times at increasing aging times, and this is seen in isothermal aging experiments [30–33]. This effect is less pronounced in Fig. 6(a) because the measurements were performed as a function of temperature essentially resulting in a complicated aging profile. However, isothermal dynamic measurements can show clearly the effect of physical aging on the relaxation spectrum in both mechanical and dielectric measurements. This is outside the scope of the current research, here we are concerned with fitting the experimental data of PMMA over a wide temperature range and using this to calculate the distribution of relaxation times and observe any effect of thermal treatment.

5. Discussion: comparison between the experimental data and the model

Here, we give a direct comparison between the model and the PMMA data obtained at 1 Hz. In Fig. 8 we give a direct comparison between the EFS model and the experimental data of the reference sample of the PMMA. Fig. 8(a) shows the loss modulus $E''(T)$ as a function of the storage modulus $E'(T)$ (Cole–Cole diagram) after a temperature scan at 1 Hz from −80 to 130 °C. Fig. 8(b) gives both the calculated and experimental δ vs. E_d curves for the reference sample of PMMA. The EFS model calculation is in good agreement with the

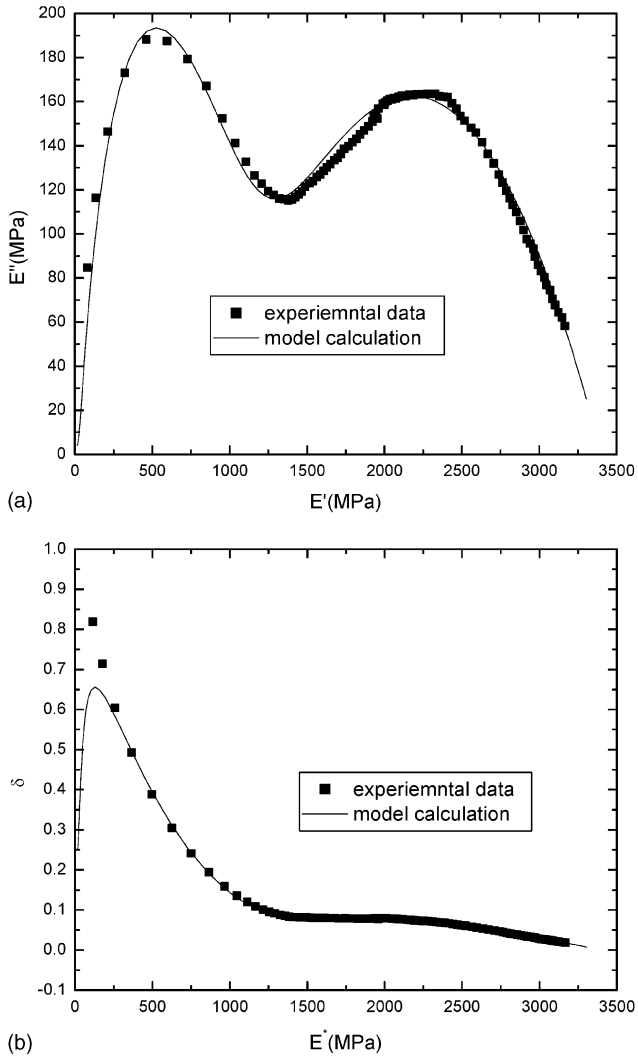

Fig. 8. (a) Comparison in the complex plane (Cole–Cole diagram) between the EFS model calculation and the experimental data of the reference PMMA sample. (b) Phase angle δ vs. complex modulus E^* at 1 Hz for the reference PMMA sample and the EFS model calculation.

experimental data of PMMA over a wide temperature range. It is clear that this model can fit well both the secondary and primary relaxation β and α of PMMA. The model parameters used to fit the data are listed in Table 2.

Table 2
The EFS model parameters used to fit the data of the reference PMMA sample

a	0.33
b	0.79
c	0.17
E_{0_1} (MPa)	1
E_{0_2} (MPa)	1
E_{u_1} (MPa)	2400
E_{u_2} (MPa)	970
τ_a (s)	200
τ_b (s)	1200
τ_c (s)	4×10^{-6}

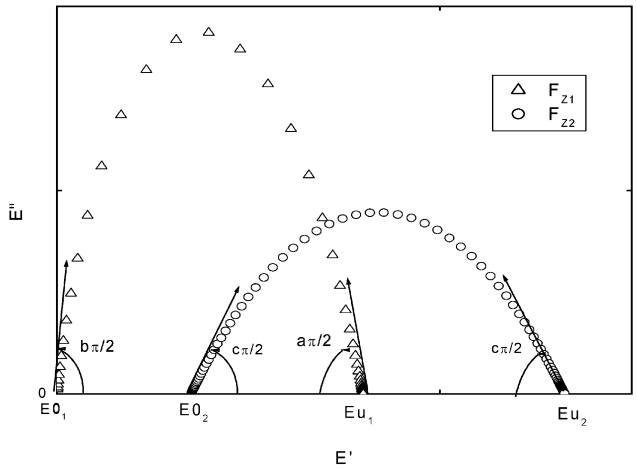

Fig. 9. The Cole–Cole diagram showing the determination of the EFS model parameters.

A fitting procedure was used to obtain a single set of parameters describing the Cole–Cole diagram shown in Fig. 9. The relaxed E_0 ($= E_{0_1} + E_{0_2}$) and non-relaxed E_u ($= E_{u_1} + E_{u_2}$) moduli are determined from the Cole–Cole diagram of the experimental data (see Fig. 3). In this case the parameters E_{0_1}, E_{0_2}, E_{u_1} and E_{u_2} were adjusted to the experimental value of E_0 and E_u. It is important to note that that the maximum of the β relaxation is very sensitive to the c parameter whereas the maximum of the α relaxation is related to the a parameters. These maxima are relatively insensitive to the time constant τ_a and τ_b. These times vary with the frequency and depend on the reference temperature under isothermal conditions [34, 23]. Based on the time–temperature superposition principle, Huet [34] observed that the ratio $\theta = \left(\frac{\tau_b}{\tau_a}\right)^{-b}$ is constant for a given reference temperature. The values of the parameters c, τ_c, were adjusted by least squares fitting to the Cole–Cole diagram (E'' vs. E') and to δ vs. E^* plot. In addition, the E_u, E_0, parameters are extrapolated from the Cole–Cole diagram of the experimental data. Iterating the procedure did not improve the fit.

Fig. 10(a) and (b) show the comparison between the model calculation and experimental data of the aged sample of PMMA. Fig. 10(a) shows the Cole–Cole diagram whereas Fig. 10(b) shows the comparison between the calculated and experimental δ vs. E^* plots. For the aged sample, we followed the above procedure where the c, τ_c and θ parameters were simultaneously varied to give a better fit. The model parameters used to fit the data of the aged sample are provided in Table 3. It can be seen that the b parameter is not affected by the thermal treatment of the sample because this parameter characterizes only the viscoelastic properties of polymers above the glass transition temperature i.e. b is related to the slope in the high temperature region of the Cole–Cole diagram. In the same way the c parameter is almost constant for the reference and the aged samples because c is related to the low temperature region far below the glass transition (i.e. c is the slope in the β relaxation region of the Cole–Cole diagram).

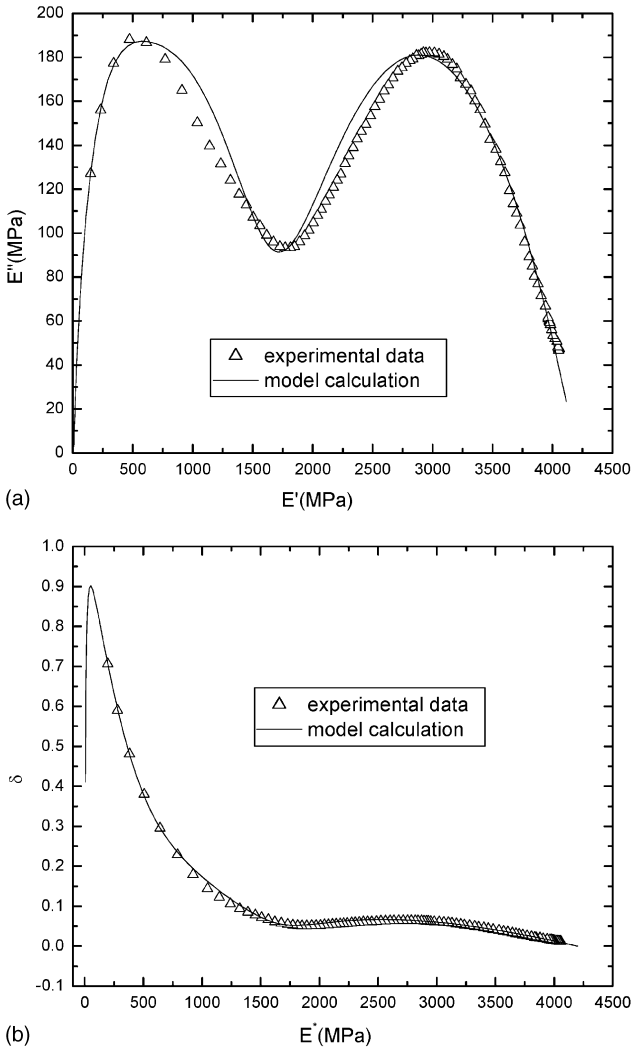

Fig. 10. (a) Comparison in the complex plane (Cole–Cole diagram) between the EFS model calculation and the experimental data of the aged PMMA sample. (b) Phase angle δ vs. complex modulus E^* at 1 Hz for the aged PMMA sample and the EFS model calculation.

The calculated relaxation spectra $H(\tau)$ corresponding to the reference and the aged samples of PMMA are shown in Fig. 11. The model parameters used to calculate the spectra are the same as those shown in Tables 2 and 3. The spectrum

Table 3
The EFS model parameters used to fit the data of the aged PMMA sample

a	0.23
b	0.79
c	0.175
E_{0_1} (MPa)	1
E_{0_2} (MPa)	1
E_{u_1} (MPa)	2650
E_{u_2} (MPa)	1600
τ_a (s)	150
τ_b (s)	5000
τ_c (s)	10^{-9}

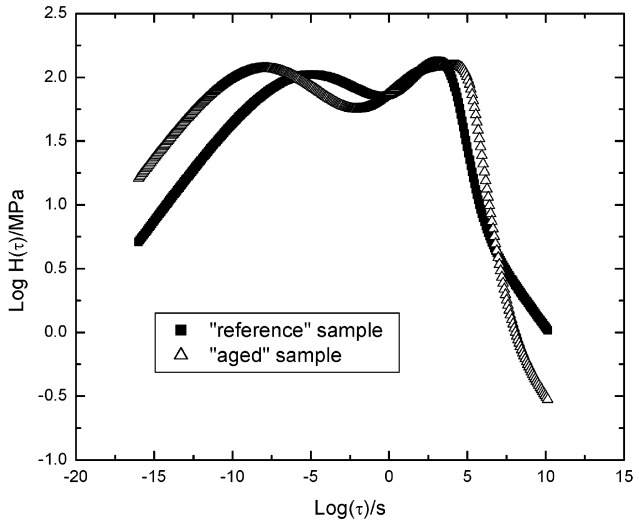

Fig. 11. Comparison between the relaxation spectra $H(\tau)$ of the reference and the aged samples of PMMA.

$H(\tau)$ shows two maxima corresponding to the β and α relaxations and covering more than 20 decades in time. We note that the peak of the β relaxation is broader than that for the α relaxation. It is clear that the spectrum of the aged sample is different from that of the reference sample. Little shift of the spectrum in time scale is observed in the vicinity of the α relaxation. However, in this study we cannot observe the normal physical aging shift on the relaxation spectrum as is seen for the isochronal experiments discussed earlier. Struik [30] observed that the creep compliance shifts to longer times at increasing aging time and suggested that this is due to a shift of the retardation spectrum without any shape change. The same trend was observed by many authors when performing isothermal physical aging after a down jump in temperature from above to below the glass transition [31,33,35]. Recent results have shown the same trend when performing creep experiments after carbon dioxide pressure jumps from above to below the glass transition pressure [36].

Further experiments and modeling work should be performed using dielectric spectroscopy, in part to model the data over a wide frequency range and also to see the effect of physical aging on the relaxation spectrum. It remains to be shown that during isothermal physical aging at high frequencies, the relaxation spectrum could be shifted to longer times.

6. Conclusions

In this paper, we studied the distribution of relaxation times of amorphous polymers from the glassy state to the glass transition region. The continuous relaxation spectrum $H(\tau)$ was calculated from the EFS model that we have developed in previous work [24,25]. This spectrum was calculated using the properties of the inverse Stieljes integral transformation [2]. The distribution of relaxation times $H(\tau)$ is dependent on three non-integer parameters a, b and c whose values are between 0 and 1. In the case of the reference sample of PMMA, the a, b and c parameters were approximately 0.3, 0.8 and 0.17, respectively.

In addition, we have studied the effect of thermal treatment (physical aging) on the relaxation spectrum for an aging time of 20 h after temperature down jumps from above T_g to 70 °C. The experiments were performed by DMTA under isochronal conditions at 1 Hz over a range of temperature from −80 to 130 °C. The relaxation spectrum calculated from the model covers more than 20 decades of time and follows the shape of the loss modulus. The broadness of the spectrum $H(\tau)$ is slightly changed during physical aging and a small shift in the spectrum to longer relaxation times was observed.

The models discussed in our work can be regarded as an interesting generalization, especially for materials showing complex behavior. However, more experiments in dielectric spectroscopy should be performed to observe the effect of physical aging and frequency on the model parameters and also on the relaxation spectrum.

Importantly, the approach to the analysis of dynamic data presented here shows the potential of the fractional calculus method to determine the relaxation spectrum $H(\tau)$. An extensive and systematic study of physical aging phenomenon associated with $H(\tau)$ deserve to be realized and should certainly be very rich in new conclusions.

Acknowledgements

One of the authors (Mataz Alcoutlabi) would like to thank Dr P. A. O'Connell from the Chemical Engineering Department at Texas Tech University for stimulating discussions concerning this work.

References

[1] Ferry JD. Viscoelastic behavior of polymers. New York: Wiley; 1980.
[2] Tschoegl NW. The phenomenological theory of linear viscoelastic behavior, an introduction. New York: Springer-Verlag; 1988.
[3] Oldham KB, Spanier J. The fractional calculus. New York: Academic Press; 1974.
[4] Bagley RL, Torvik PJ. J Rheol 1983;27:201.
[5] Hilfer R, editor. The application of fractional calculus in physics. Singapore: World Scientific; 2000.
[6] Metzler R, Klafter J. J Non-Cryst Solids 2002;305:81.
[7] Koeller RC. J Appl Mech 1984;51:299.
[8] Friedrich C. Lecture notes in physics 1991;381:321.
[9] Friedrich C, Braun H. Rheol Acta 1992;31:309.
[10] Glöckle RC, Nonnenmacher TF. Macromolecules 1991;24:6426.
[11] Heymans N, Bauwens J-C. Rheol Acta 1994;33:210.
[12] Schiessel H, Blumen A. J Phys A: Math Gen 1993;26:5057.
[13] Schiessel H, Blumen A. Macromolecules 1995;28:4013.
[14] Sokolov IM, Klafer J, Blumen A. Phys Today 2002;55:48. Nov.
[15] Heymans N. Rheol Acta 1996;35:508.
[16] Hilfer R. J Non-Cryst Solids 2002;305:12.

[17] Hilfer R. Phys Rev E 2002;65:061510.
[18] Hilfer R. J Phys: Condens Matter 2002;14:2297.
[19] Hilfer R. Chem Phys 2002;284:399.
[20] Davidson W, Cole R. J Chem Phys 1951;19:1484.
[21] Williams G, Watts D. Trans Faraday Soc 1970;66:80.
[22] Havriliak S. J Polym Sci 1966;14:99.
[23] Cole KS, Cole RH. J Chem Phys 1941;2:341.
[24] Alcoutlabi M, Martinez-Vega JJ. Polymer 1998;39:6269.
[25] Alcoutlabi M, Martinez-Vega JJ. J Mater Sci 1998;34:2361.
[26] Booj CH, Thoone GPJM. Rheol Acta 1992;21:15.
[27] Martinez-Vega JJ, Trumel H, Gacougnolle JL. Polymer 2002;43:4979.
[28] Muzeau E. 'Etude des relaxations mécaniques α et β du PMMA, du PS et de leurs copolymères' Thesis. INSA de Lyon 1992; p. 221.
[29] Tordjeman P, Tézé L, Halary JL, Monnerie L. Polym Eng Sci 1997;37:1621.
[30] Struik LCE. Physical ageing in amorphous polymers and other materials. Amsterdam: Elsevier; 1978.
[31] Hutchinson JM. Prog Polym Sci 1995;20:703.
[32] McKenna GB. Glass formation and glassy behavior. In: Booth C, Price C, editors. Comprehensive polymer science. Polymer properties, vol. 2. Oxford: Programon; 1989. p. 311.
[33] O'Connell PA, McKenna GB. Polym Eng Sci 1997;37:1485.
[34] Huet C. Thesis. University of Paris: France, 1963.
[35] Lee A, McKenna GB. Polymer 1988;29:1812.
[36] Alcoutlabi M, Briatico-Vengosa F, McKenna GB. J Polym Sci Part B, Polym Phys 2002;40:2050.